J. Fluid Mech. (1999), *vol.* 393, *pp.* 1–21. Printed in the United Kingdom

On the suppression of shock-induced separation in Bethe–Zel'dovich–Thompson fluids

By M. S. CRAMER AND S. PARK

Engineering Science and Mechanics, Virginia Polytechnic Institute and State University, Blacksburg, VA 24061-0219, USA

(Received 27 November 1995 and in revised form 10 March 1999)

We consider the reflection of oblique compression waves from a two-dimensional, steady, laminar boundary layer on a flat, adiabatic plate at free-stream pressures such that dense-gas effects are non-negligible. The full Navier–Stokes equations are solved through use of a dense-gas version of the Beam–Warming implicit scheme. The main fluids studied are Bethe–Zel'dovich–Thompson (BZT) fluids. These are ordinary gases which have specific heats large enough to cause the fundamental derivative of gasdynamics to be negative for a range of pressures and temperatures in the single-phase vapour regime. It is demonstrated that the unique dynamics of BZT fluids can result in a suppression of shock-induced separation. Numerical tests performed reveal that the physical mechanism leading to this suppression is directly related to the disintegration of any compression discontinuities originating in the flow. We also demonstrate numerically that the interaction of expansion shocks with the boundary layer produces no adverse effects.

1. Introduction

An important loss mechanism in many transonic and supersonic flows is caused by shock-induced boundary layer separation. In addition to significant losses, such separations can set up self-sustained oscillations and therefore may give rise to vibration and noise. In the present investigation we examine one of the most elementary shock–boundary layer interactions, namely that caused by the reflection of an oblique shock from a rigid surface. Such interactions are prevalent in aerodynamic applications and can also occur in supersonic turbomachinery flows. Here we consider a class of fluids of general interest as working fluids for so-called organic Rankine cycles and demonstrate that the natural dynamics of such gases can reduce and even eliminate shock-induced separation.

The physical mechanism leading to shock-induced separation is due to the strong adverse pressure gradient carried by the incident compression shock. The adverse pressure gradient decelerates the low-momentum flow in the boundary layer and if the gradient is strong enough, a backflow, i.e. separation, region can occur. An inspection of even the incompressible Navier–Stokes equations or of the classical Faulkner–Skan flows reveals that it is the magnitude of the spatial gradients, rather than the overall pressure change, which gives rise to separation. Explicit formulas relating the pressure gradient to the onset of separation can be found in the well-known references by Schlichting (1968) and White (1974).

An example which is easily reproduced, is closely related to the main work of the present study, and which illustrates the influence of the pressure gradient on

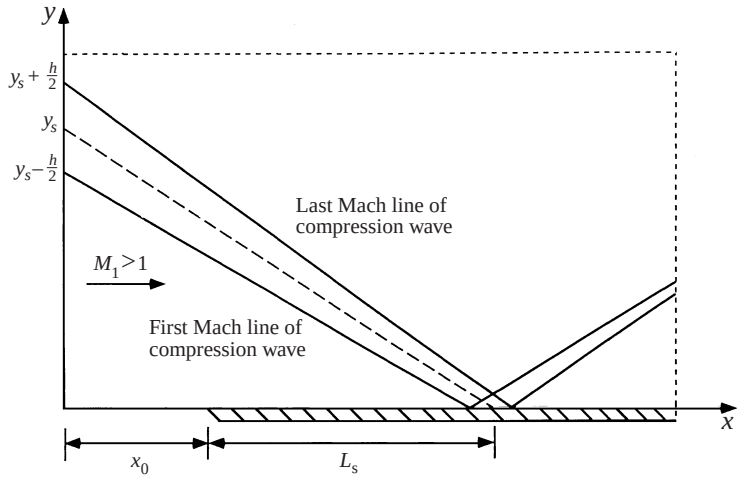

FIGURE 1. Configuration for numerical test of the effect of the width of the incoming compression wave.

the boundary layer has been computed by Park (1994). A schematic of the flow is depicted in figure 1. The numerical scheme and general configuration are identical to those used later in the present study; full details are given in §§ 2–4. In this example, the physical problem is that where a sequence of incoming compression waves of increasing width are reflected from a laminar flat-plate boundary layer. In each case the fluid is air at a free-stream Mach number, pressure, and temperature of 2.0, 0.134 atm, and 308.6 K. Because the pressures are well below those of the thermodynamic critical point, the flow behaviour is that of a perfect gas. The strength of each incident compression wave was fixed so that the flow deflection angle was 2.5°. The local Reynolds number at the wave impingement point was 2.96×10^5. The first wave considered was a shock initiated at a distance y_s above the plate. The other two waves were smooth waves initiated at the same distance upstream of the plate but were of width h centred on the initiation point of the shock. In the case of the shock the impingement point was estimated by the oblique shock relations. In the case of the smooth waves, the impingement point was taken to be the point at which the first Mach wave strikes the plate. The resultant skin friction coefficient c_f has been plotted in figure 2. Because of the difference in definitions of the impingement point, the scaling factor L_s will be different for the case involving the shock and the cases involving smooth waves; this will cause a slight distortion and shifting of the profile in the streamwise direction.

It is seen that the shock is strong enough to separate the laminar boundary layer as evidenced by the region of $c_f < 0$ on the plate. When the initial width of the compression wave is 36% of the value of y_s, the degree of separation, as measured by the size of the skin friction coefficient, appears to be reduced. In the final case, the total initial width of the incoming compression wave was 72% of y_s. Inspection of the skin friction variation plotted in figure 2 reveals that the adverse pressure gradient in this case is so weak that the boundary layer remains attached. Because the overall pressure rise resulting from the reflection has the same value for each case, this series of examples gives further evidence for the idea that the likelihood of separation depends on the width of the incident waves, i.e. on the strength of the adverse pressure gradient, in addition to the value of the total pressure rise.

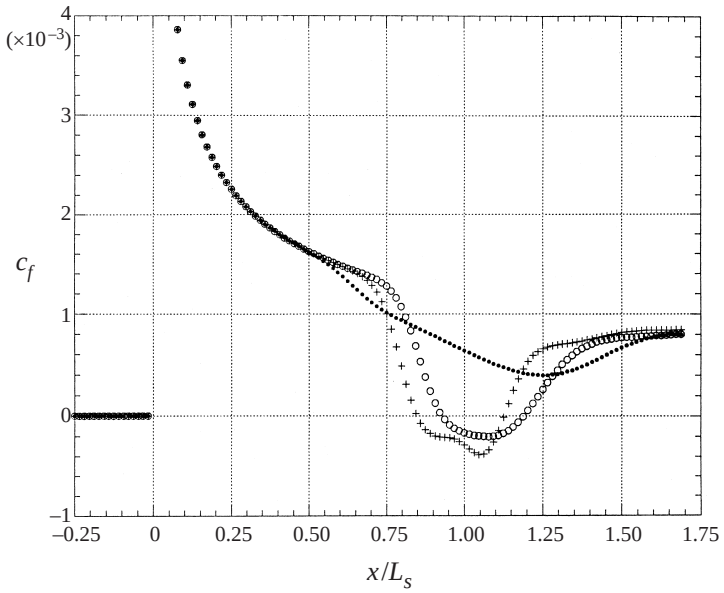

FIGURE 2. Variation of skin friction for three compression waves in low-pressure air. The flow deflection angle of each wave was 2.5°. The plus symbols correspond to a compression shock initiated at $x = 0, y = y_s$. The open and solid circles denote compression waves having initial width $h = 0.36y_s$ and $h = 0.72y_s$, respectively.

Most of our intuition regarding compressible flows and therefore shock–boundary layer interaction is based on the perfect gas theory. This gas model is an excellent approximation when the pressures and densities are sufficiently low. However, in high-pressure applications, the perfect gas model may not yield accurate predictions of the actual gas response. More complex equations of state such as the van der Waals, Redlich–Kwong, and Beattie–Bridgeman equations must then be employed. Discussions of these well-known models can be found in most texts on engineering thermodynamics, e.g. Jones & Hawkins (1986). When such high-pressure corrections to the ideal-gas equation of state are required we will refer to the fluid as a dense, in contrast to a dilute or low-pressure, gas.

Applications where high-pressure, i.e. dense-gas, effects must be considered include the design of subcritical and supercritical power cycles (Reynolds & Perkins 1977 and Jones & Hawkins 1986) and chemical and fuel transport (Leung & Epstein 1988 and Bober & Chow 1990). Further examples include the design of hypersonic and transonic wind tunnels as described by Enkenhus & Parazzoli (1970), Wagner & Schmidt (1978), Simeonides (1987, 1990), Anderson (1991*a*, *b*), and Anders (1993). Dziedzic *et al.* (1993) described the use of supercritical hydrogen to cool hypersonic aircraft. A summary of the non-classical heat transfer in near-critical CO_2 has been given by Hall (1971) and Hsu & Graham (1976).

Recent studies have revealed that the dynamics of dense gases can differ significantly from those of low-pressure gases, particularly when fluids other than air and water are employed. Bethe (1942) and Zel'dovich (1946) were the first to point out that the qualitative behaviour of compressible flows depends on the sign of the thermodynamic parameter

$$\Gamma \equiv \frac{a}{\rho} + \left.\frac{\partial a}{\partial \rho}\right|_s, \tag{1.1}$$

where ρ and s are the fluid density and entropy and

$$a \equiv \left(\frac{\partial p}{\partial \rho}\bigg|_s \right)^{1/2} \tag{1.2}$$

is the thermodynamic sound speed. The parameter (1.1) is frequently referred to as the fundamental derivative of gasdynamics. The more recent studies of Cramer (1991*a*, *b*), Cramer & Best (1991), and Cramer & Crickenberger (1992) reveal that qualitative, but less dramatic, differences may also be observed when $0 < \rho\Gamma/a < 1$.

The value of (1.1) for perfect gases, i.e. gases satisfying the ideal gas law and the condition of constant specific heats, is given by

$$\Gamma = \frac{a}{\rho}\frac{\gamma+1}{2},$$

where γ is the ratio of specific heats. Because $\gamma > 1$ for all real gases, $\rho\Gamma/a > 1$ whenever the perfect gas approximation is valid. It turns out that any fluid having $\rho\Gamma/a > 1$ exhibits the same qualitative behaviour as a perfect gas. The full range of values which can be attained by the fundamental derivative are illustrated in figure 3 where (1.1) has been evaluated for a range of commercially available heat transfer and Rankine-cycle working fluids. In each case the temperature corresponds to that at the thermodynamic critical point of the fluid in question. The gas model is that developed by Martin & Hou (1955); full details of its implementation can be found in § 3. The main point of interest in these plots is that the scaled value of the fundamental derivative of most fluids has a local minimum at one-half to two-thirds of the critical density. In figure 3 and in the remainder of this paper, the subscript c will denote properties evaluated at the thermodynamic critical point. This local minimum usually corresponds to values of $\rho\Gamma/a$ between zero and one. However, some of the heavier heat transfer fluids have a local minimum which corresponds to $\Gamma < 0$. This trend is seen to be in complete agreement with the work of Lambrakis & Thompson (1972), Thompson & Lambrakis (1973), and Cramer (1989). The dynamics of such negative-Γ fluids are the principal focus of the present study. Because of the contributions of the earliest investigators, we will refer to any substance having $\Gamma < 0$ for a finite range of pressures and temperatures in the single-phase regime as Bethe–Zel'dovich–Thompson (BZT) fluids. For a more complete discussion of the class of fluids of the BZT type we refer the reader to the above-mentioned articles by Bethe, Thompson and Zel'dovich, as well as the more recent reviews of Cramer (1989, 1991*a*) and Menikoff & Plohr (1989).

One of the most striking phenomena associated with BZT fluids is due to the fact that compression shocks violate the entropy inequality whenever $\Gamma < 0$ everywhere in the flow of interest. As a result, any compression discontinuity inserted in such a flow will disintegrate to form a centred compression fan analogous to the well known Prandtl–Meyer expansion fans of the perfect gas theory. The inadmissibility of compression shocks in negative-Γ fluids was first pointed out by Bethe (1942) and Zel'dovich (1946). Centred compression fans in the context of steady and unsteady flows of BZT fluids were first described by Thompson (1971) and Wendroff (1972). Although compression shocks disintegrate in flows having $\Gamma < 0$ everywhere, expansion shocks, i.e. shocks for which the pressure of a material particle decreases, not only form naturally as a result of nonlinear steepening but also satisfy all the relevant admissibility conditions. A complete discussion of the fundamental existence conditions can be found in the recent reviews of Menikoff & Plohr (1989) and Cramer (1991*a*).

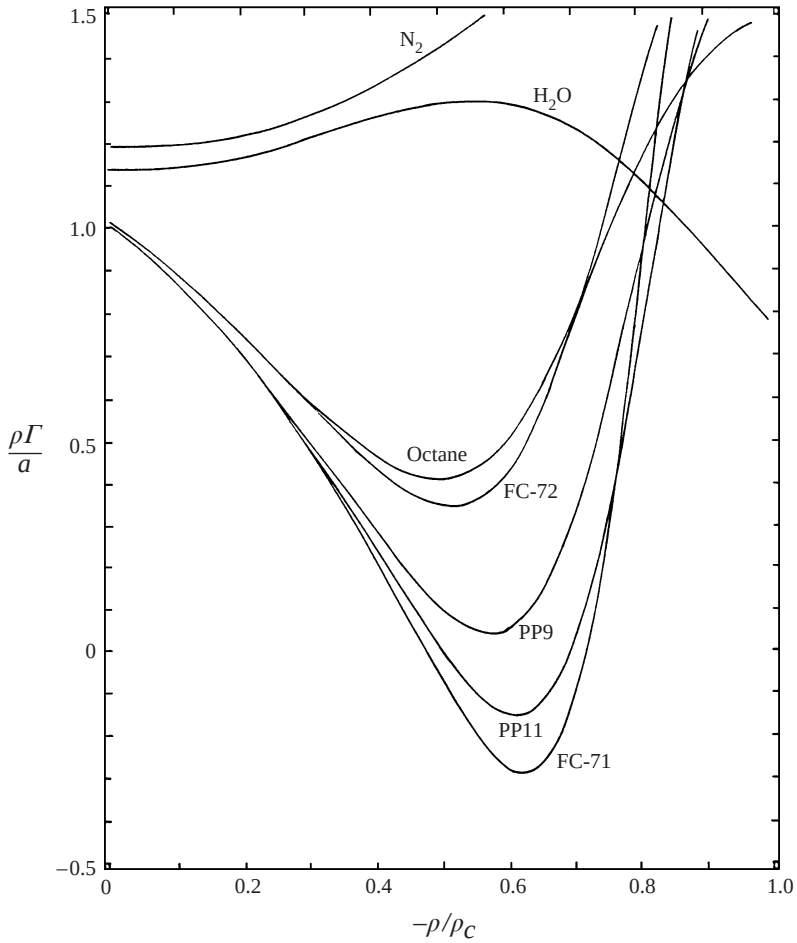

FIGURE 3. Variation of $\rho\Gamma/a$ along the critical isotherm of each fluid. The gas model in each case is that due to Martin & Hou (1955) with a power-law specific heat.

The motivation for the study of the shock-induced separation in BZT fluids becomes clear when we recall that it is both the strength and the width of the incoming wave which gives rise to separation. Even if a compression discontinuity is introduced into a supersonic flow of a $\Gamma < 0$ fluid, the natural dynamics will be such that the original discontinuity will arrive at other boundaries, e.g. other turbine blades, in the form of a wave of non-zero width. The resultant pressure gradient experienced by the boundary layer will be significantly decreased and it may turn out that the boundary layer can remain attached. The goal of the present investigation is to examine whether such a suppression of shock-induced separation can in fact be attained.

A first step toward understanding the dense-gas viscous–inviscid interaction was accomplished by Kluwick (1994) who extended the classical triple-deck analysis to include not only gases at high pressure but also those of the BZT type. In the case of purely supersonic flows, the gasdynamic nonlinearity was found to be negligible for the purposes of analysing the interaction region; this of course is consistent with the conclusions of the classical theory. Thus, for a given incoming (inviscid) signal, we expect no new physics in the interaction zone. We feel this result suggests that any

suppression of separation will be due to the differences in the width of the incoming compression wave. The Navier–Stokes computations of the present study are seen to be consistent with this conclusion.

A second contribution of Kluwick (1994) is that he delineated the appropriate form of the scaling laws for arbitrary, rather than perfect, gases. In particular, all of the perfect gas scalings carry over immediately to the case of arbitrary gases provided only that the pressure is measured by the pressure coefficient

$$c_p \equiv \frac{p - p_1}{\frac{1}{2}\rho_1 a_1^2 M_1^2}, \tag{1.3}$$

where M is the Mach number and the subscript 1 denotes the free-stream conditions, and that the wall shear stress $T_{yx}|_w$ be measured by the skin friction coefficient

$$c_f \equiv \frac{T_{yx}|_w}{\frac{1}{2}\rho_1 a_1^2 M_1^2}. \tag{1.4}$$

As an example, we note that the pressure distribution in the interaction region can be written

$$c_p = \frac{\left(c_{f1}\right)^{1/2}}{\left(M_1^2 - 1\right)^{1/4}} P(\tilde{x}), \tag{1.5}$$

where c_{f1} is the skin friction immediately upstream of the interaction region and P is the same function of the scaled x-variable ($\tilde{x}$) as is found in the classical, i.e. perfect gas, theory.

An important parameter in any study of shock–boundary layer interaction is the overall pressure rise required for separation. Here we combine the estimate of Katzer (1989) with scaling laws of Kluwick (1994) to obtain

$$\frac{c_{pT}\left(M_1^2 - 1\right)^{1/4}}{\left(c_{f1}\right)^{1/2}} > 2.6 \tag{1.6}$$

as the criterion for separation. Here c_{pT} is the pressure coefficient associated with the total pressure rise resulting from the reflection. As pointed out by Katzer (1989) the numerical factor on the right-hand side of (1.6) can vary from author to author in the general range of 2 to 3. As an example we consider the shock–boundary layer interaction corresponding to figure 2. The above ratio was found to be

$$\frac{c_{pT}\left(M_1^2 - 1\right)^{1/4}}{\left(c_{f1}\right)^{1/2}} \approx 4.02$$

which is consistent with the criterion (1.6). Further numerical comparisons using the same numerical scheme as described here were carried out by Cramer, Park & Watson (1997). This study revealed that Kluwick's extension of the triple-deck theory to dense gases agrees well with Navier–Stokes solutions of the shock-boundary layer interaction problem.

The same physics which causes the disintegration of compression discontinuities in $\Gamma < 0$ fluids also gives rise to the formation of expansion shocks. A natural question when considering the use of BZT fluids in applications is whether such expansion shocks can have deleterious effects upon interaction with boundary layers. Kluwick (1994) has also addressed this issue in the context of the triple-deck theory. His conclusions were that the interaction should resemble that corresponding to an

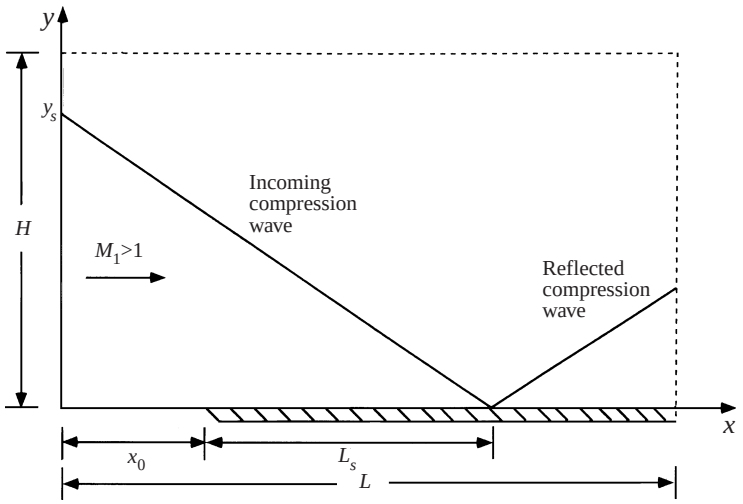

FIGURE 4. Coordinate system and computational domain for the numerical calculations.

expansion discontinuity in a perfect gas. As a result, expansion shocks will also not increase the likelihood of separation. In the present study we provide verification for this claim through use of our Navier–Stokes code.

In § 2 we record the full set of Navier–Stokes equations employed in the present study and in § 3 we describe the gas models and fluid properties used. The numerical scheme and the various consistency checks employed are described in § 4. Our primary results are given in § 5.

2. Formulation

In the present study, we restrict our attention to steady, two-dimensional flow of a Navier–Stokes fluid. Body forces and heat sources will be neglected and the flow is regarded as being single phase, in equilibrium and sufficiently far from the thermodynamic critical point; it is this set of assumptions which permits us to model the fluid as a Navier–Stokes fluid. The x- and y-coordinate axes are depicted in figure 4. The origin is taken to be at some arbitrary distance x_0 upstream of the flat plate, the positive x-axis is in the direction of the undisturbed flow, and the y-direction is transverse to the incoming flow.

In the implementation of the numerical scheme described in § 4, the unsteady form of the Navier–Stokes equations will be required. When these equations are written in conservative form, we have

$$\frac{\partial \boldsymbol{Q}}{\partial t} + \frac{\partial \boldsymbol{F}}{\partial x} + \frac{\partial \boldsymbol{G}}{\partial y} = \frac{\partial \boldsymbol{F}_v}{\partial x} + \frac{\partial \boldsymbol{G}_v}{\partial y}, \tag{2.1}$$

where

$$\boldsymbol{Q} = \begin{Bmatrix} \rho \\ \rho u \\ \rho v \\ E \end{Bmatrix}, \quad \boldsymbol{F} = \begin{Bmatrix} \rho u \\ \rho u^2 + p \\ \rho uv \\ u(E+p) \end{Bmatrix}, \quad \boldsymbol{G} = \begin{Bmatrix} \rho v \\ \rho uv \\ \rho v^2 + p \\ v(E+p) \end{Bmatrix}, \tag{2.2}$$

and

$$\boldsymbol{F}_v = \begin{Bmatrix} 0 \\ T_{xx} \\ T_{xy} \\ w_x \end{Bmatrix}, \quad \boldsymbol{G}_v = \begin{Bmatrix} 0 \\ T_{yx} \\ T_{yy} \\ w_y \end{Bmatrix}. \tag{2.3}$$

The quantities u and v are the x- and y-components of the fluid velocity, p and ρ are the fluid pressure and density, and

$$E \equiv \rho \left(e + \frac{u^2 + v^2}{2} \right). \tag{2.4}$$

Here the thermodynamic quantity e is the thermal energy; thus, (2.4) will be referred to as the total energy per unit volume. The quantities T_{xx}, $T_{yx} = T_{xy}$, T_{yy} are the Cartesian components of the Navier–Stokes stress tensor which can be written

$$\left.\begin{aligned} T_{xx} &= (\lambda + 2\mu) \frac{\partial u}{\partial x} + \lambda \frac{\partial v}{\partial y}, \\ T_{xy} &= T_{yx} = \mu \left(\frac{\partial u}{\partial y} + \frac{\partial v}{\partial x} \right), \\ T_{yy} &= (\lambda + 2\mu) \frac{\partial v}{\partial y} + \lambda \frac{\partial u}{\partial x}, \end{aligned}\right\} \tag{2.5}$$

where μ and λ are the shear and second viscosities which satisfy

$$\mu \geqslant 0, \quad \mu_b \equiv \lambda + \tfrac{2}{3}\mu \geqslant 0; \tag{2.6}$$

μ_b is the bulk viscosity. The quantities w_x and w_y are the energy fluxes defined as

$$w_x \equiv T_{xx}u + T_{xy}v - q_x, \quad w_y = T_{yx}u + T_{yy}v - q_y, \tag{2.7}$$

where $\boldsymbol{q} = -k\nabla T$ is the Fourier heat flux vector, T is the absolute temperature, and

$$k > 0 \tag{2.8}$$

is the thermal conductivity. The first two terms in each of (2.7) represent the work done per unit time by the stress tensor. The first row of (2.1) is recognized as the mass equation, the second and third rows are the two components of the momentum equation, and the fourth row is the energy equation.

The plate is taken to be adiabatic, impenetrable, and located at $y = 0$, $x > x_0$, where x_0 is the location of the leading edge of the plate. As a result, the physical boundary conditions at the plate can be written

$$u = v = \frac{\partial T}{\partial y} = 0 \quad \text{for} \quad y = 0, x > x_0. \tag{2.9}$$

The flow far upstream, i.e. as $x \to -\infty$, is taken to be uniform with velocity components $u = U_1 > 0, v = 0$. The flow velocity U_1 is such that the incoming flow is supersonic. Here we restrict our attention to reflections which leave the flow supersonic; thus, for the present purposes, Mach reflections will be ignored.

3. Gas models

A full specification of any single-phase gas requires a knowledge of the functions

$$p = p(\rho, T) \quad \text{and} \quad c_{v\infty} = c_{v\infty}(T), \tag{3.1}$$

and

$$\mu = \mu(\rho, T), \quad \lambda = \lambda(\rho, T), \quad k = k(\rho, T), \tag{3.2}$$

where $c_{v\infty}(T)$ is the low-pressure, i.e. the ideal gas, specific heat at constant volume. In the usual way we will refer to the first of (3.1) as the equation of state. In the present investigation we employ the equation of state proposed by Martin & Hou (1955). The advantages of this model are that it is widely employed in engineering practice and it has a strong analytical basis so that only a minimum number of experimental parameters are required for its use. The Martin–Hou equation agrees well with the measured properties of light substances such as nitrogen and steam. Good agreement is also found when comparisons can be made to the heavier fluids of interest in studies of BZT fluids. The work of Thompson & Lambrakis (1973) and Cramer (1989) has also shown that it appears to be conservative with respect to predictions of negative nonlinearity. Details of the implementation of the Martin–Hou equation can be found in the articles by Martin & Hou (1955) and Cramer (1989).

The ideal-gas specific heat will be modelled by a power law of the form

$$c_{v\infty}(T) = c_{v\infty}\left(T_{ref}\right)\left(\frac{T}{T_{ref}}\right)^{n}, \tag{3.3}$$

where T_{ref} is a reference temperature, and n is a material-dependent exponent. The advantage of (3.3) is its simplicity and accuracy over the temperature ranges of interest in the present study. The values of $c_{v\infty}(T_{ref})$ and n are typically estimated by fitting (3.3) to empirical data or more complex models. Details of the fitting procedure for the heavier fluorocarbons are described by Cramer (1989).

Once the temperature dependence of the ideal-gas specific heat and the full form of the equation of state (3.1) are known, all other thermodynamic parameters can be determined through use of the standard identities found in most texts on thermodynamics.

In the dense gas regime, the variation of the transport properties (3.2) with both density and temperature will be important. In the present investigation we employ the dense-gas shear viscosity and thermal conductivity models developed by Chung, Lee & Starling (1984) and Chung *et al.* (1988). The key characteristics of these models are similar to the Martin–Hou equation. That is, they have a strong analytical basis, require only a minimum amount of physical data, and they reduce to standard ideal-gas formulas in the low-pressure limit. Furthermore, the comparisons provided by Reid, Prausnitz & Poling (1987) reveal reasonable accuracy in the dense gas regime.

Finally, the bulk viscosity (2.6) must be specified. The authors know of no bulk viscosity data for light fluids in their high-pressure regime nor appropriate data for the heavier hydro- and fluorocarbons of interest here. Throughout, we will simply take the ratio μ_b/μ to be a numerical constant. It should be noted that errors in the value of the bulk viscosity are not likely to have a significant effect on the results. In the lowest-order approximation of the boundary layer, the viscous–inviscid interaction region (as described by triple-deck theory), and the inviscid flow, the bulk viscosity is seen to be negligible. The only influence of μ_b is expected to be in the description of the interior of shock waves. Numerical trials reported by Park (1994) have verified that reasonable variations in the value of μ_b have essentially no effect on the complete viscous–inviscid interaction.

In order to ensure that the flow is single phase, the final pressures and temperatures were checked against the Riedel (1954) vapour-pressure correlation. If any point was found to be in the two-phase regime, the whole calculation was rejected.

As pointed out above, each model for the equation of state, ideal-gas specific heat, transport properties, and the phase boundary require only a minimum number of physical data. The required quantities include the values of the pressure, temperature, and specific volume at the thermodynamic critical point, the boiling temperature, the molecular weight, the acentric factor, and the dipole moment of the molecule. The acentric factor is a macroscopic measure of the acentricity of the molecule and is zero for spherical molecules such as those of monatomic gases. The definition of this factor may be found in Reid *et al.* (1987) which reveals that it may be computed directly from vapour-pressure data and the critical properties. The dipole moment is a measure of the polarity of the molecule and is zero for non-polar substances. When polar substances such as steam, ammonia, acids, alcohols, and freons are considered, two more empirical constants are required. These are discussed below when the modelling of steam is considered. It is important to note that our original restrictions to single-phase, equilibrium Navier–Stokes flows permits us to use a gas model which determines the pressure and the transport properties uniquely in terms of the density and temperature. As a result, no new length scales are introduced into the problem. The issues of boundary layer similarity and scalings for the interaction zone remain the same as in the perfect gas theory.

The main Navier–Stokes computations described in §§ 1, 4, and 5 involve air at low pressure, steam, PP11 ($C_{14}F_{24}$), and FC-71 ($C_{18}F_{39}N$). In the remainder of this Section, we summarize the basis for the choices of the relevant physical parameters. The actual numerical values are tabulated by Park (1994).

Most of the data for air were taken from Rohsenow, Harnett & Ganic (1985). The dipole moment was taken to be zero and the acentric factor was taken to be that of N_2, i.e. 0.039. The bulk viscosity was taken to be 0.6μ as suggested by Truesdell (1953). Because the specific heat of air is nearly constant over a wide range of temperatures, we have taken $n = 0$ in the calculations involving air in §§ 1 and 4.

The physical data for steam are also well-established. Most of the relevant parameters were taken or estimated from those provided by Jones & Hawkins (1986) and Reid *et al.* (1987). Because water is a polar substance, the shear viscosity and thermal conductivity models of Chung *et al.* (1984, 1988) require a so-called association factor and a second parameter related to the self-diffusion coefficient of water. Both parameters were chosen to be the values given by Chung *et al.* (1984) in their Tables I and II. No data for the bulk viscosity of water vapour are available at either low or high pressure. Here we simply set the ratio $\mu_b/\mu = 1$. Specific tests conducted by Park (1994) show negligible variation in the resultant skin friction, wall pressure, and wall temperature values as μ_b ranges from 0 to 5μ.

The bulk of the data for the heat transfer fluids FC-71 and PP11 were taken or estimated from the manufacturers' (3-M Corporation and Imperial Smelting Corporation) technical publications. A detailed discussion of the estimation procedures and results for the critical properties, boiling temperature, and specific heat data is found in the article by Cramer (1989). Private communication between the first author (M.S.C.) and the manufacturers' representatives indicates that PP11 and FC-71 are non-polar so that the dipole moment was taken to be zero for each fluid. No data for the bulk viscosity of either PP11 or FC-71 exist and we took $\mu_b/\mu = 5$ for each fluid.

4. Numerical scheme

The Navier–Stokes equations (2.1)–(2.8) are solved by the Beam–Warming (1978) implicit scheme adapted to allow for the dense-gas equation of state and transport

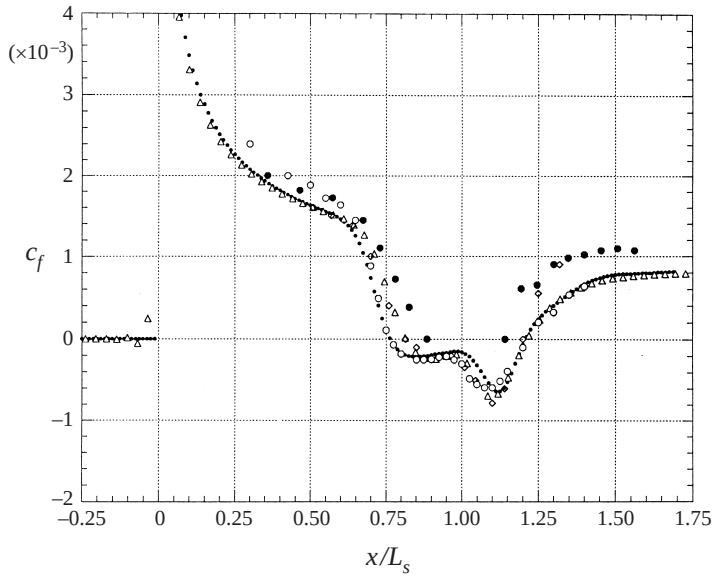

FIGURE 5. Comparison of the results of the present scheme with experiments of Hakkinen *et al.* (1959) and other computations. Large solid circles denote the experimental results, small solid circles denote the results of the present scheme, open circles denote the computations of Zhong (1994), diamonds denote the computations of MacCormack (1982) and triangles denote the computations of Walters (1994). Free-stream data and grid sizes are provided in table 1.

laws. Explicit second- and fourth-order artificial viscosities were added to reduce oscillations at the shocks. The advantage of this scheme is that it is well known and can be immediately extended to imperfect gases. Full details of its implementation in the present application and the non-dimensionalization scheme employed are given by Park (1994).

To minimize the computation time without sacrificing accuracy, a grid clustered in the direction transverse to the plate was employed. The mapping between the physical and computational domain is given by

$$\xi = \frac{x}{L}, \quad \eta = 1 - \ln\left\{\frac{\beta + 1 - y/H}{\beta - (1 - y/H)}\right\} \Bigg/ \ln\left\{\frac{\beta + 1}{\beta - 1}\right\},$$

where $\xi = \xi(x)$ and $\eta = \eta(y)$ are the non-dimensional computational variables, β is the clustering parameter satisfying $\beta > 1$, and L and H are the dimensions of the computation domain in the flow and transverse directions, respectively. Typical values of β were between 1.002 and 1.003. As a result, the number of points across the boundary layer at the shock impingement point was approximately 20–40.

The computational domain is depicted in figure 4. The shock was introduced either at the inflow boundary ($x = 0$) or at the upper boundary ($y = H$). At each of these boundaries, the flow variables were fixed at either the free-stream conditions or the conditions after the incident shock; the latter conditions were computed from an iterative solution to the oblique shock relations similar to that described by Cramer (1991*b*). At the right-hand boundary, second-order extrapolated outflow conditions were imposed. At the lower boundary ($y = 0$), either symmetry conditions or the physical boundary conditions were applied as appropriate.

Extensive numerical checks and comparisons with known solutions have been

Reference	p_1(atm)	T_1(K)	M_1	p_3/p_1	Grid sizes
Present work	0.134	308.6	2	1.4	156×101
Walters (1994)	0.133	293	2	1.4	62×113
MacCormack (1982)	*	*	2	1.4	32×32
Zhong (1994)	*	*	2	1.4	102×144
Hakkinen *et al.* (1959)	*	*	2	1.4	N/A

TABLE 1. Data of free-stream conditions, pressure rise, and grids corresponding to figure 5. The * indicates that no explicit statement of the thermodynamic properties were given. However, it is believed that these were at low pressure and room temperature. The subscripts 1 refer to quantities evaluated in the free stream and the subscript 3 denotes quantities evaluated after reflection.

carried out by Park (1994). A comparison of the results of our computations with the experimental data of Hakkinen, Greber & Trilling (1959) is presented in figure 5. The computed results of MacCormack (1982), Zhong (1994), and R. W. Walters (private communication, 1994) are also included. The free-stream conditions and shock pressure rise are listed in table 1. The grid size employed by each investigator is also reported. Inspection of figure 5 reveals reasonable agreement of our computations with those of previous authors. Because the free-stream pressures are on the order of one atmosphere or less, we regard these comparisons to be evidence that our dense-gas version of the Beam–Warming scheme recovers the perfect-gas results in the low-pressure limit.

Park (1994) has compared the results of the present scheme to the detailed computations of dense-gas boundary layers reported by Whitlock (1992), Cramer & Whitlock (1993), and Cramer, Whitlock & Tarkenton (1996). In these studies a standard finite difference scheme was applied to the dense-gas version of the compressible boundary layer equations. Mach numbers ranging from zero to 3 and free-stream pressures ranging from one atmosphere to slightly supercritical values were reported. Whitlock's results were found to be in excellent agreement with Anderson's (1991*a*) Navier–Stokes computations of compressible, dense-gas boundary layers on flat plates (private communication with S. T. Whitlock). Excellent agreement between Park's results and those of Whitlock was reported which provides partial verification of the implementation of the numerical scheme and the dense-gas viscosity and thermal conductivity models.

The authors are not aware of any computations of the present kind which involve shock–boundary layer interactions in dense gases. The interactions presented by Wagner & Schmidt (1978) correspond to a free-stream pressure of one bar. The Navier–Stokes computations of Anderson (1991*a*) involve transonic flow and nearly normal shocks on airfoils; as result, no direct comparisons are appropriate. However, Cramer *et al.* (1997) have verified that the numerical scheme described here agrees well with the scaling laws of the dense-gas triple-deck theory developed by Kluwick (1994). The cases considered included free-stream pressures corresponding both perfect-gas and dense-gas flows.

On the basis of the comparisons discussed above, we conclude that the dense-gas version of the Beam–Warming scheme is capable of describing the flows of interest in the present investigation.

Extensive tests were also made by Park (1994) to determine the grid refinement required to render the computed results independent of the grid size. It was found that ξ vs. η grids in the range of 125×76 to 187×101, depending on the fluid, were

adequate to ensure that the grid size no longer influenced the results, although even more refined grids were typically used. In any case, any comparisons were made using identical grids. Furthermore, all cases presented here were checked for iterative convergence. It is expected, although not formally guaranteed, that any observed differences are due to the physics rather than differences in numerical error.

5. Results

The first comparison to be made is that between steam and FC-71. The former is chosen because it is a non-BZT fluid which is commonly employed in heat transfer and Rankine cycle applications. The latter (FC-71) is a BZT fluid with a critical temperature approximately equal to that of steam. The following comparison will be direct in the sense that the behaviour of both steam and FC-71 will be evaluated at equivalent flow conditions.

We first consider the flow of steam at a free-stream pressure, temperature, and Mach number equal to 8.55 atm, 646.15 K, and 2.0, respectively. The flow deflection angle carried by the incident shock was 3° and the position at which the incident shock strikes the plate corresponds to a local Reynolds number of 2.96×10^5. This local Reynolds number is based on the free-stream conditions and L_s is defined to be the distance from the leading edge to the shock impingement point as computed by the oblique shock relations for pressurized gases. An outline of the development of these shock relations was given by Cramer (1991*b*). The computed skin friction and wall pressure coefficients are plotted in figures 6(*a*) and 6(*b*). Inspection of figure 6(*a*) reveals that the incident shock is strong enough to separate the laminar boundary layer; the separation zone extends from approximately $0.8L_s$ to $1.18L_s$. In fact, the skin friction plot exhibits the classical double minimum profile suggesting that separation is well-established and not marginal.

We next consider the flow of the BZT fluid FC-71 at exactly the same free-stream Mach number, pressure, and temperature as for the steam. Furthermore, the flow deflection angle of the incident compression wave is also taken to be 3°. Thus, the geometry generating the compression can be said to be identical for both fluids. It is both intuitively obvious and suggested by the detailed analysis of Kluwick (1994) that the appropriate measure of the strength of the reflection is the increase in the pressure coefficient (1.3). It is easily demonstrated that this quantity will then be identical for each flow, at least according to linear theory. For the stated free-stream conditions and flow deflection angle the upstream and downstream values of the scaled fundamental derivative $\rho\Gamma/a$ were found to be -0.04 and -0.16, respectively. The fundamental shock existence conditions described by Menikoff & Plohr (1989) and Cramer (1991*a*) can be employed to show that this compression discontinuity is inadmissible. Furthermore, it is easily verified that the original discontinuity will disintegrate into a centred isentropic compression fan. Because this compression wave arrives at the boundary layer with a non-zero width, the definition of the impingement Reynolds number must be reconsidered. In order to make a meaningful comparison, we choose the initiation point of the compression wave to be such that the local Reynolds number at the approximate centre of the wave is equal to that used in the calculation involving steam, i.e. 2.96×10^5. The location of the position of the centre of the wave impingement region was estimated as that predicted by the numerical solution to the exact oblique shock relations for the inadmissible discontinuity. It is easily shown that the computed impingement point of the inadmissible shock will always lie between the impingement points of the first and last Mach waves

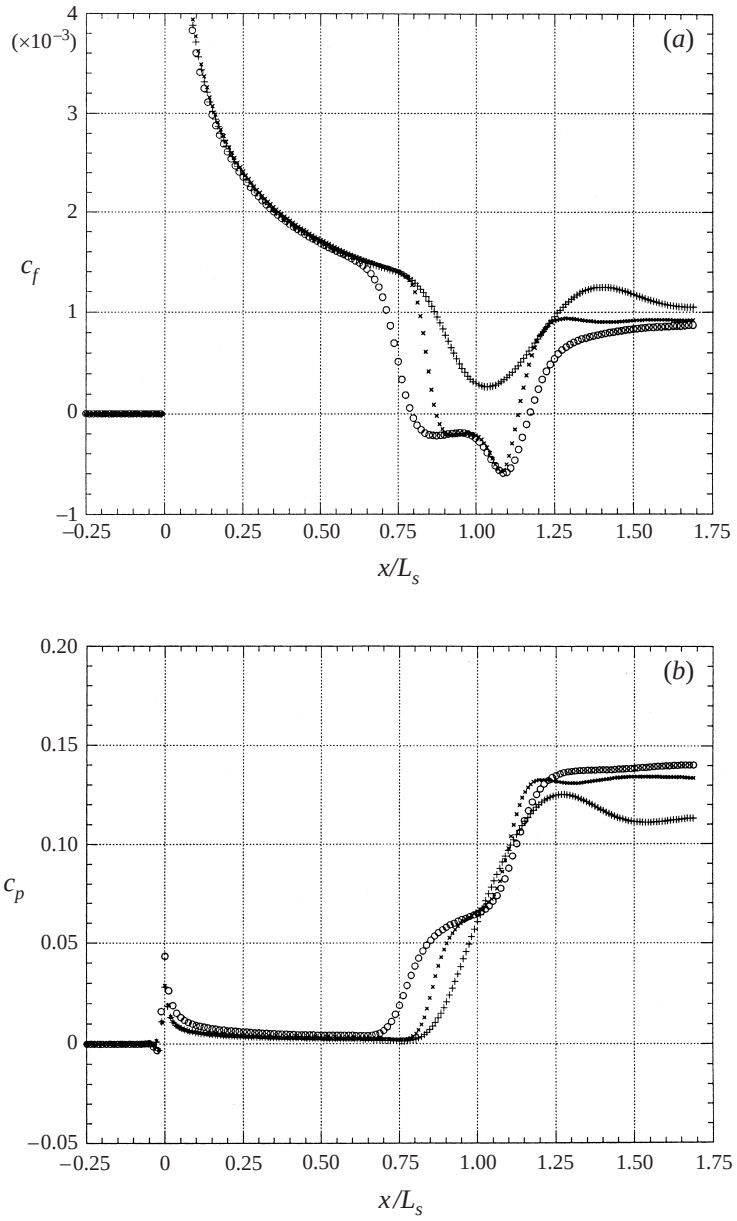

FIGURE 6. (*a*) Skin friction and (*b*) pressure coefficient variation for compression waves in steam and FC-71. The flow deflection angle carried by each compression wave is 3° and the free-stream Mach number and temperature are 2.0 and 646.15 K. The open circles correspond to steam at $p_1 = 8.55$ atm, the plus symbols denote FC-71 at the same pressure as steam and the cross symbols denote FC-71 at $p_1 = 1$ atm.

of the actual centred fan, at least when $\Gamma < 0$ both upstream and downstream of the proposed discontinuity. In fact, weak shock theories of the type described by Cramer (1991*a*) and Crickenberger (1991) can be used to show that the inadmissible discontinuity always bisects the resultant centred fan. This result is recognized as the $\Gamma < 0$ counterpart of the bisection rule described in many texts on gasdynamics; see e.g. Whitham (1974).

Inspection of figures 6(*a*) and 6(*b*) reveals that the interaction of the centred fan in FC-71 results in an attached boundary layer. The minimum skin friction is seen to be approximately 3×10^{-4} whereas that for steam is seen to be approximately -6×10^{-4}. Coincidentally, this large difference in the minimum skin friction is approximately the same as that seen in the comparisons between the shock and the isentropic compression wave depicted in figure 2. Numerous tests indicate that the results have converged and that the grid sizes (218×101 for FC-71 and 156×101 for steam) used were adequate to ensure that the results are independent of the grid. We therefore conclude that the observed suppression of separation is of physical rather than numerical origin.

The variation of the pressure coefficient plotted in figure 6(*b*) shows that the total change in c_p during the reflection involving FC-71 is slightly less than that of steam. This difference is due to the fact that the compression in FC-71 is isentropic whereas that in steam involves an increase in entropy. Similar differences between compression fans and compression shocks were seen in the Euler computations of Monaco (1994). When the separation parameter of (1.6) is computed it is found that

$$c_{pT}\left(M_1^2-1\right)^{1/4}/\left(c_{f1}\right)^{1/2} \approx 4.78 \quad \text{for steam and} \approx 4.01 \text{ for FC}-71.$$

As expected, both values are well above those needed to produce separation. We also note that the value for FC-71 is approximately that recorded for the shock-induced separation seen in figure 2.

In order to demonstrate that the suppression of separation in FC-71 is due to the novel dynamics associated with the $\Gamma < 0$ regime and not to the particular choice of FC-71, we have computed a case where the free-stream state of FC-71 corresponds to a nearly perfect gas. The free-stream temperature, free-stream Mach number, the flow deflection angle of the incident shock, and the impingement Reynolds number were all taken to be identical to those of steam. The only difference between this case and those already discussed is that the free-stream pressure was taken to be 1 atm instead of 8.55 atm. The values of $\rho\Gamma/a$ ahead of and behind the incident shock were both found to be approximately 1.0; this value is to be expected given the large values of the ideal-gas specific heat of FC-71. As in the case of steam the resultant compression discontinuity can be shown to be admissible and arrives at the boundary layer as a discontinuity, at least according to the inviscid theory. The skin friction and wall pressure coefficient have been plotted in figure 6(*a*, *b*). Because the incoming signal is now a shock and the scaled strength parameter

$$\frac{c_{pT}\left(M_1^2-1\right)^{1/4}}{\left(c_{f1}\right)^{1/2}} \approx 4.76,$$

the boundary layer is seen to separate with approximately the same minimum pressure coefficient as obtained for steam. The main difference between the skin friction variations is the apparent width of the separation zone. However, this difference is due to the scaling of x with L_s, chosen to ensure that the impingement Reynolds numbers of steam and FC-71 were identical. Because the Mach numbers were also matched, the values of L_s will be different for different fluids. In particular, it is the differences in the factor $\mu/\rho a$ which cause the differences in L_s.

The results of this comparison strongly suggest that the suppression of separation in FC-71 is due to the unique dynamics of BZT fluids in their $\Gamma < 0$ regime. A detailed inspection of the incoming boundary layer as well as similar inspections of dense-gas boundary layers computed by Whitlock (1992) reveal no unusual dynamics

in the viscous flow regime. We therefore conclude that the main physical reason for the suppression of separation in BZT fluids is due to the non-zero width of the incoming compression wave which in turn is due to the disintegration of compression discontinuities in the $\Gamma < 0$ regime.

To further illustrate the effect of the width of the compression fan on the boundary layer we consider the flow of FC-71 at exactly the same free-stream pressure (8.55 atm), temperature (646.15 K) and Mach number (2.0) as used in our comparison between steam and FC-71. The initiation point of the compression discontinuity was chosen so that the approximate impingement Reynolds number was again 2.96×10^5 and the transverse distance from the plate was identical to that used in the previous example involving steam and FC-71. The only difference is that the flow deflection angle of the incident wave was taken to be 6.5° instead of 3°. The free-stream value of $\rho\Gamma/a$ is of course identical to that of the previous example involving FC-71, i.e. -0.04, and the value of $\rho\Gamma/a$ after the discontinuity was found to be -0.06. As in the previous example, the discontinuity can be shown to be inadmissible; as a result it naturally disintegrates into a centred fan. The resultant skin friction and wall pressure coefficient variations are plotted as open circles in figure 7(a, b). Although the wave strikes the boundary layer as a fan, the strength of the overall compression is over twice as large as that of the previous example of a compression fan. As is evident from figure 7(a), the pressure rise is large enough to separate the boundary layer.

It is of interest to note that the relation between the flow deflection angle θ_2 carried by the incident fan and the incident wave strength and wave width (Δx) can be approximated by

$$c_{p2} \approx \frac{2\theta_2}{\sqrt{M_1^2 - 1}} \quad \text{and} \quad \Delta x \approx -\frac{M_1^4}{M_1^2 - 1}\frac{\rho_1 \Gamma_1}{a_1}\theta_2 \Delta y, \tag{5.1}$$

where c_{p2} is the pressure coefficient immediately following the fan as estimated by the linear simple-wave theory and Δy is the distance between the initiation point of the fan and the plate measured transverse to the flow. The second of (5.1) can be obtained from a $\rho\Gamma/a = O(1)$ version of the weak shock theory of Crickenberger (1991) or Cramer (1991a) or by a small-disturbance approximation of Thompson's (1971) expression for the Mach angle in an isentropic simple wave:

$$\frac{\mathrm{d}\psi}{\mathrm{d}\theta} = \frac{\rho\Gamma}{a}\frac{M^2}{M^2 - 1},$$

where ψ is the exact (convected) Mach angle and M is the local Mach number. By an inspection of (5.1) we conclude that, as the flow deflection angle (θ_2) increases, both the strength and width increase at approximately the same rate. A comparison of figures 6(a) and 7(a) suggests that the effect of the increase in strength on the separation condition dominates that of the increase in width which in turn results in the observed flow separation.

To isolate the effect of the width of the incoming wave we have computed the flow of FC-71 under exactly the same free-stream conditions and impingement Reynolds number as the case depicted by open circles in figure 7(a, b), with exactly the same inadmissible compression discontinuity but the initiation point of the compression discontinuity in the present case is located at a transverse distance which is 61% farther from the plate. As a result, the compression wave striking the plate boundary layer is 61% wider than that of the previous case. The results for the skin friction and wall pressure coefficient are plotted in figure 7(a, b) as cross symbols, which reveals that the increase in the initiation distance and therefore the increase in final wave

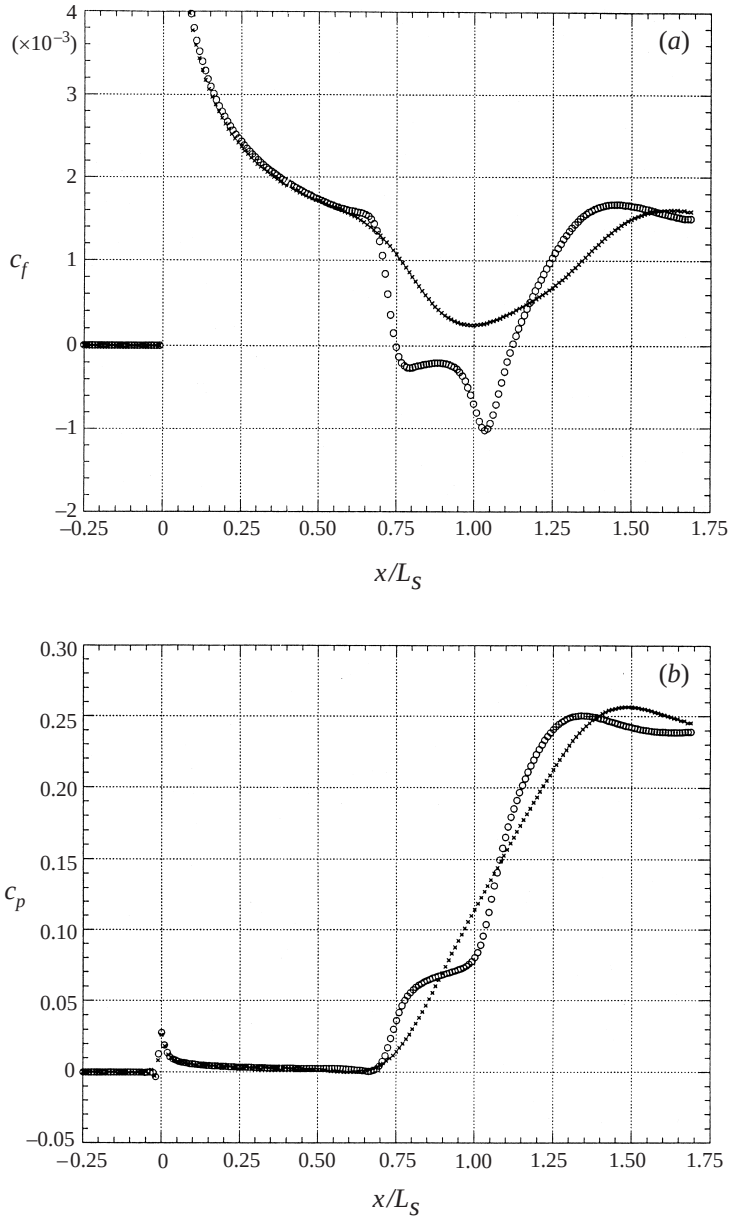

FIGURE 7. Effect of compression fan width on (*a*) skin friction and (*b*) pressure coefficient in FC-71 for flow deflection angle 6.5°, free-stream Mach number 2.0, free-stream pressure 8.55 atm and impingement Reynolds number 2.96×10^5. The cross symbols denote a fan which has been initiated at a transverse distance which is 61% farther from the plate than the case depicted by open circles.

width is sufficient to attach the flow. With respect to the task of isolating the effect of wave width, we regard the comparison seen in figure 7(*a*, *b*) to be more direct than that between steam and FC-71 because all parameters except the width were held fixed in the former. In this sense this comparison is closely related to that done for air in § 1. Because all viscous effects are expected to be identical in the examples

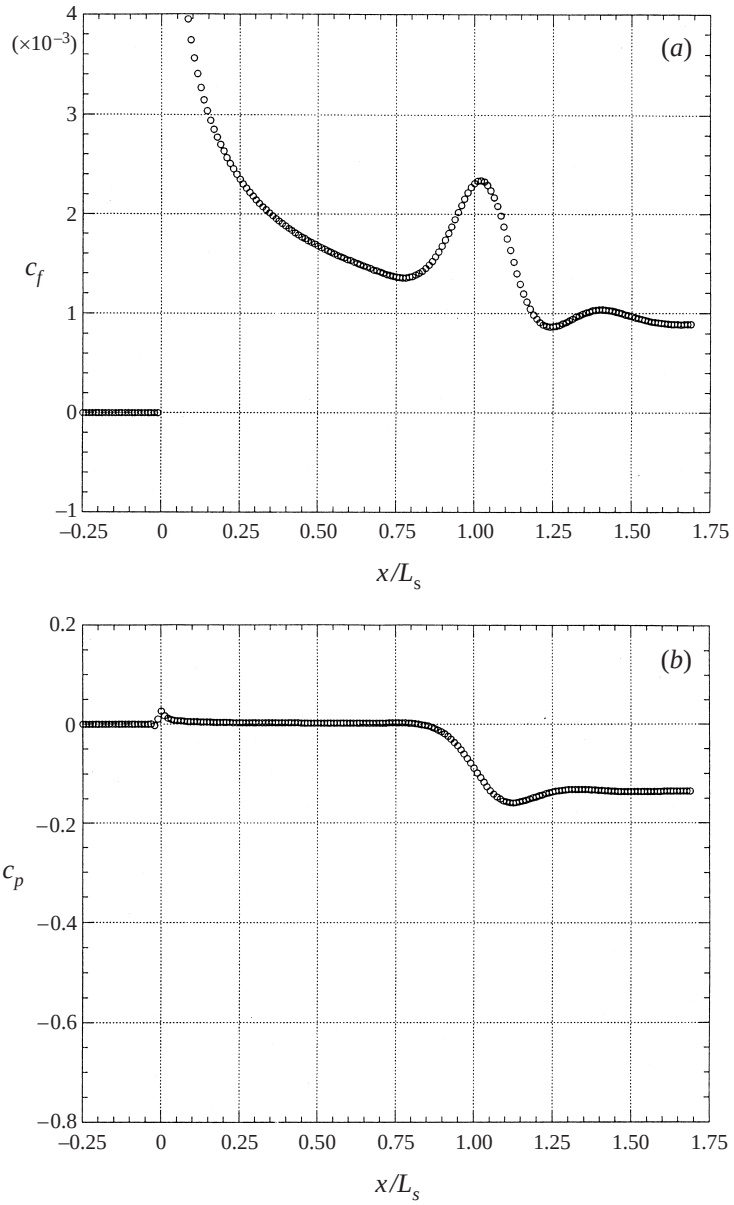

FIGURE 8. (*a*) Skin friction and (*b*) pressure coefficient corresponding to the interaction of an admissible expansion shock with a boundary layer in PP11. The free-stream pressure, temperature, and Mach number are 13.8 atm, 648.85 K, and 2.0 respectively.

illustrated by figure 7(*a*, *b*), these comparisons provide further strong evidence for the idea that the observed suppression of separation is caused by differences in the incoming signal which in turn is due to the unique *inviscid* dynamics of BZT fluids.

As a final example of shock–boundary layer interaction in BZT fluids we consider the case of the collision of an expansion shock with a boundary layer. The fluid is PP11 at a free-stream pressure, temperature, and Mach number of 13.8 atm, 648.85 K, and 2.0, respectively. The initiation point of the wave was taken to be such

that impingement Reynolds number was again 2.96×10^5. The flow deflection angle was taken to be -3° which is, of course, consistent with the generation of an expansion wave. The value of $\rho\Gamma/a$ in the free stream was -0.20 and the value immediately after the expansion discontinuity was found to be -0.12. Under these conditions it can be shown that this discontinuity is admissible and therefore propagates as a shock wave. The variation of the skin friction and wall pressure coefficient are plotted in figures 8(*a*) and 8(*b*). Inspection of the first of these figures reveals that the expansion shock causes the skin friction to increase in the interaction region. The observation that expansion shocks cause no difficulties with respect to separation is consistent with the remarks of Kluwick (1994) as well as reasoning based on the perfect-gas theory.

A second example of the interaction of an admissible expansion shock with a laminar boundary layer in FC-71 and somewhat different free-stream conditions was presented by Park (1994). His results are completely consistent with those plotted here.

6. Summary

The primary goal of the present investigation was to examine viscous–inviscid interactions in BZT fluids. This was done by generating numerical solutions to the full Navier–Stokes equations for the well-understood benchmark problem of the reflection of an oblique shock from a laminar boundary layer on a flat plate. The main result is the demonstration that the use of BZT fluids in the $\Gamma < 0$ regime can suppress boundary layer separation. The evidence presented here as well as the analytical work of Kluwick (1994) strongly suggests that the primary physical reason for this suppression is the disintegration of compression discontinuities at temperatures and pressures corresponding to $\Gamma < 0$. As a result, the incident compression wave is of non-zero width which represents a decrease in the adverse pressure gradient carried by the wave. If the decrease in the pressure gradient is large enough for a given strength of the compression wave, the boundary layer is able to remain attached during the interaction. A similar mechanism for the suppression of separation was observed in the example involving air and depicted in figures 1 and 2. Thus, the key to understanding the suppression mechanism is the non-classical dynamics of BZT fluids in the inviscid portion of the flow.

An advantage of the discovery of this relatively simple physical mechanism is that much of our perfect-gas intuition regarding the viscous–inviscid interaction can be carried over to BZT fluids with little or no modification. The main effort to reduce separation will therefore be to control the inviscid portion of the flow.

We have also verified Kluwick's (1994) prediction that the interaction of expansion shocks with boundary layers causes no new difficulties with respect to separation. This conclusion is consistent with the idea that the non-classical physical effects are primarily observed in the inviscid part of the flow.

The separation criterion (1.6) is clearly violated when the disintegration of the compression discontinuity results in an attached boundary layer. However, condition (1.6) only holds when the incoming signal is a discontinuity rather than a smooth compression. As a result, it is not appropriate to conclude that triple-deck theory, in its most general sense, is invalid. In fact, the authors believe that an important task for future studies is the development of a modified triple-deck analysis which can describe compression waves of non-zero width; a reasonable approach would be similar to that given by El-Mistikawy (1994). The main goal of such an analysis

would be to provide the modified separation condition for BZT fluids. In addition, the scaling laws for the dependence on the wave width would be clearly delineated. When the triple-deck results are combined with the weak shock theory of Cramer (1991*a*) and Crickenberger (1991) or Euler computations similar to those of Monaco (1994), design strategies for the control of the inviscid flow can then be easily developed.

This research was funded by the National Science Foundation under grant number CTS-8913198. The authors would also like to thank Professor S. A. Ragab for many helpful suggestions in the area of computational methods and Professor L. T. Watson for making computer facilities available.

REFERENCES

Anders, J. B. 1993 Heavy gas wind-tunnel research at Langley Research Center. *ASME Paper* 93-FE-5.

Anderson, W. K. 1991*a* Numerical study of the aerodynamic effects of sulfur hexafluoride (SF6) as a test gas in wind tunnels. *NASA TP*-3086.

Anderson, W. K. 1991*b* Numerical study on using sulfur hexafluoride as a test gas in wind tunnels. *AIAA J.* **29**, 2179–2180.

Beam, R. M. & Warming, R. F. 1978 An implicit factored scheme for the compressible Navier–Stokes equations. *AIAA J.* **16**, 393–402.

Bethe, H. A. 1942 The theory of shock waves for an arbitrary equation of state. *Office Sci. Res. & Dev. Rep.* 545.

Bober, W. & Chow, W. L. 1990 Nonideal isentropic gas flow through converging-diverging nozzles. *Trans. ASME*: *J. Fluids Engng* **112**, 455–460.

Chung, T. H., Ajlan, M., Lee, L. L. & Starling, K. E. 1988 Generalized multiparameter correlation for nonpolar and polar fluid transport theories. *Indust. Engng Chem. Res.* **27**, 671–679.

Chung, T. H., Lee, L. L. & Starling, K. E. 1984 Application of kinetic gas theories and multiparameter correlation for prediction of dilute gas viscosity and thermal conductivity. *Indust. Engng Chem. Fundam.* **23**, 8–13.

Cramer, M. S. 1989 Negative nonlinearity in selected fluorocarbons. *Phys. Fluids* A **1**, 1984–1987.

Cramer, M. S. 1991*a* Nonclassical dynamics of classical gases. In *Nonlinear Waves in Real Fluids* (ed. A. Kluwick), pp. 91–145. Springer.

Cramer, M. S. 1991*b* On the Mach number variation in steady flows of dense hydrocarbons. *Trans. ASME*: *J. Fluids Engng* **113**, 675–680.

Cramer, M. S. & Best, L. M. 1991 Steady, isentropic flows of dense gases. *Phys. Fluids* A **3**, 219–226.

Cramer, M. S. & Crickenberger, A. B. 1992 Prandtl-Meyer function for dense gases. *AIAA J* **30**, 561–564.

Cramer, M. S., Park, S. H. & Watson, L. T. 1997 Numerical verification of scaling laws for shock-boundary layer interactions in arbitrary gases. *Trans. ASME*: *J. Fluids Engng* **119**, 67–73.

Cramer, M. S. & Whitlock, S. T. 1993 Similarity laws in dense gas flows. *ASME Paper* 93-FE-6.

Cramer, M. S., Whitlock, S. T. & Tarkenton, G. M. 1996 Transonic and boundary layer similarity laws in dense gases. *Trans. ASME*: *J. Fluids Engng* **118**, 481–485.

Crickenberger, A. B. 1991 The dynamics of steady supersonic dense gas flows. MS Thesis, Virginia Polytechnic Institute and State University, Blacksburg, Virginia.

Dziedzic, W. M., Jones, S. C., Gould, D. C. & Petley, D. H. 1993 Analytical comparison of convective heat transfer correlation in supercritical hydrogen. *J. Thermophys. Heat Transfer* **7**, 68–73.

El-Mistikawy, T. M. A. 1994 Separation prevention as an indirect problem based on the triple-deck theory. *AIAA J.* **32**, 1423–1427.

Enkenhus, K. R. & Parazzoli, C. 1970 Dense gas phenomenon in a free-piston hypersonic wind tunnel. *AIAA J* **8**, 60–65.

HAKKINEN, R. J., GREBER, I. & TRILLING, L. 1959 The interaction of an oblique shock wave with a laminar boundary. *NASA Memo* 2-18-59W.

HALL, W. B. 1971 Heat transfer near the critical point. In *Advances in Heat Transfer* (ed. T. F. Irvine & J. P. Hartnett), Vol. 7, pp. 1–86.

HSU, Y. Y. & GRAHAM, R. W. 1976 *Transport Processes in Boiling & Two-Phase Systems*. Hemisphere Series in Thermal and Fluid Engineering, McGraw-Hill.

JONES, J. B. & HAWKINS, G. A. 1986 *Engineering Thermodynamics*. McGraw-Hill.

KATZER, E. 1989 On the scales of laminar shock/boundary layer interaction. *J. Fluid Mech.* **206**, 477–496.

KLUWICK, A. 1994 Interacting laminar boundary layers of dense gases. *Acta Mechanica* **4**, 335–349.

LAMBRAKIS, K. & THOMPSON, P. A. 1972 Existence of real fluids with a negative fundamental derivative Γ. *Phys. Fluids* **5**, 933–935.

LEUNG, J. C. & EPSTEIN, M. 1988 A generalized critical model for nonideal gases. *AIChE J.* **34**, 1568–1572.

MACCORMACK, R. W. 1982 A numerical method for solving the equations of a compressible viscous flow. *AIAA J* **20**, 1275–1281.

MENIKOFF, R. & PLOHR, B. 1989 Riemann problem for fluid flow of real materials. *Rev. Mod. Phys.* **61**, 75–130.

MARTIN, J. J. & HOU, Y. C. 1955 Development of an equation of state for gases. *AIChE J.* **1**, 142–151.

MONACO, J. F. 1994 Supersonic flows of Bethe–Zel'dovich–Thompson fluids in cascade configurations. MS Thesis, Virginia Polytechnic Institute and State University, Blacksburg, Virginia.

PARK, S.-H. 1994 Viscous-inviscid interactions of dense gases. PhD Dissertation, Virginia Polytechnic Institute and State University, Blacksburg, Virginia.

REID, R. C., PRAUSNITZ, J. M. & POLING, B. E. 1987 *The Properties of Gases & Liquids*, 4th Edn. McGraw-Hill.

REIDEL, L. 1954 Eine neue Universelle Damfdruckformel-Untersuchungten über eine Erweiterung des Theorems der übereinstimmenden Zustände Teil 1. *Chem. Ing. Tech.* **26**, 83.

REYNOLDS, W. C. & PERKINS, H. C. 1977 *Engineering Thermodynamics*, 2nd Edn. McGraw-Hill.

ROHSENOW, W. M., HARNETT, J. P. & GANIC, E. N. 1985 *Handbook of Heat Transfer Fundamentals*, 2nd Edn. McGraw-Hill.

SCHLICHTING, H. 1968 *Boundary Layer Theory*. McGraw-Hill.

SIMEONIDES, G. 1987 The aerodynamic design of hypersonic contoured axisymmetric nozzles including real gas effects. *Von Karman Institute for Fluid Dynamics Tech. Mem.* 43.

SIMEONIDES, G. 1990 The VKI hypersonic wind tunnels and associated measurement techniques. *Von Karman Institute for Fluid Dynamics Tech. Mem.* 46.

THOMPSON, P. A. 1971 A fundamental derivative in gas dynamics. *Phys. Fluids* **14**, 1843–1849.

THOMPSON, P. A. & LAMBRAKIS, K. 1973 Negative shock waves. *J. Fluid Mech.* **16**, 187–208.

TRUESDELL, C. 1953 Precise theory of the absorption and dispersion of forced plane infinitesimal waves according to the Navier–Stokes equations. *J. Rat. Mech. Anal.* **2**, 643–741.

WAGNER, B. & SCHMIDT, W. 1978 Theoretical investigation of real gas effects in cryogenic wind tunnels. *AIAA J.* **16**, 580–586.

WENDROFF, B. 1972 The Riemann problem for materials with nonconvex equations of state II: General flow. *J. Math. Anal. Applics.* **38**, 640–658.

WHITE, F. M. 1974 *Viscous Fluid Flow*. McGraw-Hill.

WHITHAM, G. B. 1974 *Linear and Nonlinear Waves*. Wiley–Interscience.

WHITLOCK, S. T. 1992 Compressible flows of dense gases in boundary layers. MS Thesis, Virginia Polytechnic Institute and State University, Blacksburg, Virginia.

ZEL'DOVICH, YA. B. 1946 On the possibility of rarefaction shock waves. *Zh. Eksp. Teor. Fiz.* **4**, 363.

ZHONG, X. 1994 Application of essentially nonoscillatory schemes to unsteady hypersonic shock–shock interference heat problems. *AIAA J.* **32**, 1606–1616.